Probabilistic analysis of electromagnetic acoustic resonance signals for the detection of pipe wall thinning

Noritaka Yusa, Haicheng Song, Daiki Iwata, Tetsuya Uchimoto, Toshiyuki Takagi, Makoto Moroi

Probabilistic analysis of electromagnetic acoustic resonance signals for the detection of pipe wall thinning

Noritaka YUSA[a*], Haicheng SONG[a], Daiki IWATA[b], Tetsuya UCHIMOTO[b,c], Toshiyuki TAKAGI[b,c], Makoto MOROI[d]

a Department of Quantum Science and Energy Engineering, Graduate School of Engineering, Tohoku University, 6-6-01-2, Aramaki Aza Aoba, Aoba-ku, Sendai, Miyagi 980-8579, Japan

b Institute of Fluid Science, Tohoku University, Sendai, Japan

c ELyTMaX UMI 3757, CNRS – Université de Lyon – Tohoku University, International Joint Unit, Tohoku University, Miyagi, Japan

d Tohoku Electric Power Co., Inc., Japan

[*] Corresponding author (Noritaka Yusa)

Tel: +81-(0)22-795-6319

Fax: +81-(0)22-795-6319

Email: noritaka.yusa@qse.tohoku.ac.jp

Abstract

This study proposes a probability of detection (POD) model for the probabilistic analysis of the detectability of electromagnetic acoustic resonance (EMAR) method for the detection and evaluation of pipe wall thinning. Forty-one carbon steel plate samples with an artificially corroded groove were prepared to simulate pipe wall thinning caused by flow-assisted corrosion. Experiments were performed to gather EMAR signals from the samples, and subsequently the depths of the grooves were evaluated based on the fundamental frequency of the measured signals. The results of the experiments showed that the error in evaluating the depth of a groove tended to increase with the depth. The results also confirmed that the surface roughness of the groove would contribute to the error, and the thickness of a plate without corrosion can be quite accurately evaluated. Analyzing the measured EMAR signals using the proposed POD model, which takes these characteristics into consideration, and a conventional one confirmed that the proposed model can more reasonably evaluate the probability of detection against small wall thinning, as well as the false positive rate.

Keywords: electromagnetic non-destructive testing, electromagnetic acoustic transducer, pipe inspection, probability of detection, false positive

1. Introduction

Pipe wall thinning caused by flow-accelerated corrosion (FAC) is a major form of degradation in various industries. Pipe wall thinning can lead to a serious accident, especially if it appears in a pipe carrying high pressure or hazardous fluids like those used in power or chemical plants[1], and thus many studies have been performed to quantitatively reveal the factors affecting wall thinning rate. However, it is still challenging to predict the remaining service life of a pipe subjected to FAC accurately. Consequently, performing periodic non-destructive inspections is indispensable when evaluating pipe wall thickness so that proper maintenance actions can be taken to prevent accidents.

The commonest method to detect and evaluate pipe wall thinning is to use ultrasonic thickness gage using a straight ultrasonic beam generated by a piezoelectric transducer. However, this technique is not always economically efficient mainly because it requires a relatively long inspection time due to its manual operation, need for a couplant and surface treatment, and so on. To address this issue, the electromagnetic acoustic transducer (EMAT) has attracted attention. Whereas the pulse-echo signals of EMAT are generally less clear than those of conventional ultrasonic inspection using a piezoelectric transducer, due to the conversion of electromagnetic energy into mechanical energy, EMAT can generate ultrasonics in a wide frequency range enabling one to evaluate the thickness of targets based on resonant frequencies that can be measured with high precision using coherent detection. The application of this technique, called electromagnetic acoustic resonance (EMAR)[2]-[5], has been limited to fundamental laboratory tests mainly due to the complexity of measurement systems[6]; commercially available high-power EMAT systems have enabled studies for more practical applications[7]-[10]. Several studies have demonstrated the efficiency of EMAR in evaluating realistic pipe wall thinning[8]-[10], which concludes that EMAR can increase the efficiency of pipe inspection comparing to the conventional ultrasonic thickness gage[11].

As in other techniques, one of the practical problems in applying EMAR to the inspection of wall thinning is how to ensure the accuracy of the measurements. Recent studies have reported EMAR to be comparable to the conventional ultrasonic thickness gage and have shown that it can evaluate wall thinning with an accuracy of submicro millimeters. However, this does not mean that FAC as shallow as, for example, 0.1 mm can always be detected or that any FAC can be evaluated with an accuracy of 0.1 mm. Because of the electromechanical

coupling, EMAR signals are affected by various factors such as the surface roughness of wall thinning and the uniformity of magnetic fields on the surface of the target[12]. Evaluating the effects of all the factors is not realistic; probabilistically quantifying the uncertainty is a more reasonable approach.

One of the possible approaches to addressing this issue is the application of the concept of probability of detection (POD) that enables us to evaluate the probability of detecting a flaw as a probabilistic function of the size of the flaw[13]-[15]. Conventionally, POD has been commonly applied to analyze eddy current signals where the presence of a flaw is evaluated based on the amplitude of measured signals. Recently studies have frequently reported POD analysis of ultrasonic signals[16]-[20], most of which evaluate the presence of a flaw based on the amplitude of reflected signals. This approach would not be so reasonable to analyze signals by ultrasonic-based methods, including EMAT and EMAR, to detect wall thinning because usually no wall thinning leads to the largest signals due to the (unflawed) backwall echo. A limited number of studies have reported on POD analysis of EMAR signals due to wall thinning[21][22]; these studies adopted a conventional approach basically and thus had difficulty in evaluating the detectability against small wall thinning as described later.

On the basis of the background above, this study proposes another POD-based method to quantify the uncertainty of EMAR in evaluating wall thinning. This study prepares samples simulating FAC by artificially corroding carbon steel plates. Signals from the samples are measured using EMAR as a function of frequency, and the depths of the corrosion are evaluated based on the resonance frequencies of the EMAR signals. A POD model taking consideration of the characteristics of the signals is proposed, and analyzing the signals confirms that the model enables us to evaluate the probability of detection of shallow corrosion, and also the false positive rate, more reasonably than a conventional POD model.

2. Measuring artificial wall thinning by EMAR

2.1 Sample preparation

This study prepared S50C carbon steel plates (JIS G 4051) measuring 50 x 50 mm with a nominal thickness of 9.5 and 9.6 mm. Mechanical grooves with semi-elliptic cross-sections with a length of 50 mm, a width of 5, 10, 20, 30, or 40 mm, and a depth of 0.2, 0.5, 1.0, 1.5 or 2.0 mm were machined at the center of each plate. Vinyl tape was attached to the surface of the plate to mask area where no groove was introduced; the plates were soaked in iron(III)-chloride-based etchant H-1000A (Sunhayato Corp., Tokyo, Japan) at 50 °C for approximately 100 hours

to corrode the surface of the grooves to simulate FAC. The total number of samples prepared for this study is 41. The numbers of samples with the width of an initial groove of 5, 10, 20, 30, 40 were 5, 8, 9, 10, and 9, respectively. Figure 1 summarizes the depth and the initial width of the grooves. The depths of the grooves were deepened and widened to about 1 mm maximum by the corrosion test. No clear correlation was confirmed between the extent to which the grooves were deepened or widened and the size of the mechanically machined initial grooves. Figure 2 shows the microscopic surface profile of one of the samples measured using a laser scanning microscope VK-X1000 (Keyence Corporation, Osaka, Japan). The figure confirms that the groove has uneven rough surfaces that cannot be introduced using conventional mechanical machining.

In order to characterize the roughness of the surface of the grooves quantitatively, the heights of the surfaces of the grooves were measured using a coordinate measuring machine MCA-2 (Nikon Instech Co., Ltd., Tokyo, Japan) with a pitch of approximately 0.025mm. The measured heights were separated into high- and low-frequency components using 2D Gaussian filter with a cut-off wavelength of λ_c. to calculate the root mean square height, Sq, using the low frequency component with different λ_c. Figure 3 shows an example of how the low frequency component changes with λ_c. In most cases $\lambda_c \geqq 0.5$ mm eliminated the effect of the profile of the initial groove machined mechanically, and thus the discussion below will use Sq calculated with $\lambda_c=0.5$

2.2 Experimental setup

Figures 4 illustrates the experimental setup used in this study. The experimental setup consisted of an EMAR probe, a high power pulser-receiver, RPR-4000 (RITEC, RI, USA), an oscilloscope DPO4104 (Tektronix, OR, USA) to confirm measured signals and to perform analog-to-digital conversion, and a PC to store the signals as a function of frequency. The probe consisted of two samarium-cobalt magnets measuring $10 \times 20 \times 20$ mm and a single-layer racetrack coil, shown in Fig. 4(b), made of wire with a diameter of 0.1 mm. In the experiments the EMAR probe was situated approximately at the center of the surface of a sample where the groove was not introduced so that the long diameter of the racetrack coil was parallel to the groove. Frequencies used in the measurements ranges from 1.0 to 4.0 MHz with 500 Hz pitch.

2.3 Evaluation of the depth of the artificial wall thinning

This study evaluated the depth of a wall thinning on the basis of the resonance frequencies because frequencies satisfying a resonance condition can be directly correlated with the depth of a target as $f_n = nv/2d$, where n, v, and d are an integer, sound velocity, and the thickness of the target, respectively. Subsequently the thickness of the target is evaluated based on the fundamental resonance frequency, f_1, simply as $v/2f_1$. In this study v was set to 3,250 m/s according to the results of preliminary experiments using seven uncorroded S50C plate with a known thickness of 9.50 mm. Figure 5 presents EMAR signals due to a groove with an initial width of 5 mm. One can confirm signal peaks that periodically appear, whose interval correspond to f_1. The superposition of the n-th compression technique[10][11] was applied to quantitatively evaluate f_1.~~clarifythe fundamental resonance frequency.~~

Figure ~~6~~5 compares the true depths of the grooves measured by a dial depth gage DM-210 (TECLOCK Co., Ltd., Nagano, Japan) and the depths evaluated based on the measured EMAR signals. Whereas the true and the estimated depths are consistent with each other, the figure shows that the error in depth estimation tends to increase with the true depths.

Figures ~~6~~7-9 shows the relationships between the widths of the groove, errors in the depth evaluation, namely the difference between the evaluated and the true depths shown in Fig. ~~5~~6, and the root mean square height of the surface of the corrosion, Sq. ~~Whereas discussing their relationships quantitatively is difficult, the figure implies that the surface roughness affects the error in the depth evaluation, which would be reasonable as a rough surface should scatter ultrasonics.~~ Figures 7 and 8 show that evaluating the depths of grooves with small initial widths is accompanied by relatively large error; Fig. 9 reveals that grooves with small initial widths tend to have large roughness on their surfaces. Because the size of the magnet, which affects the ultrasonic propagating inside the target, is not too small compared with the smallest width of the grooves, it is likely that the relatively poor correlation between the evaluated and true depths when grooves have small initial widths stemmed from the surface roughness as a rough surface should scatter ultrasonics. It should be noted that discussing their relationships quantitatively would require further studies with more samples with various profiles.

3. Probabilistic analysis of EMAR results

This study attempts to evaluate the uncertainty of the capability of EMAR with the aid of the concept of POD. The conventional procedure of a POD analysis is[13][14]:

(1) measure signals ($\hat{a}$) due to many flaws with known sizes (a);

(2) transform $\hat{a}$ and a, if necessary, so that they exhibit a linear relationship with homogeneity;

(3) assume $\hat{a} = \beta_0 + \beta_1 a + N(0,\sigma^2)$, where $N(\mu,\sigma^2)$ is a normal distribution with a mean of μ and standard deviation of σ, and perform maximum likelihood analysis to estimate the parameters β_0 and β_1;

(4) decide a threshold of $\hat{a}$, $\hat{a}_{dec}$, that is sufficiently larger than noise, namely signals gathered when there is no flaw;

(5) calculate the probability that a flaw with a size of a is detected as the probability that its signal exceeds $\hat{a}_{dec}$: $POD(a)=\Phi\{(\beta_0+\beta_1 a - \hat{a}_{dec}) /\sigma\}$, where Φ represents the cumulative distribution function of the standard normal distribution.

It should be noted that this procedure has been especially successful for analyzing eddy current signals where one detects flaws based on the amplitude of measured signals. In contrast, applying the procedure to the analysis of EMAR signals to detect wall thinning leads to a few concerns such as:

- The backwall echo that appears when there is no flaw is usually larger than the echo from wall thinning, and no echo implies that an anomaly, most likely wall thinning with quite a rough surface, scatters the ultrasonics. Consequently, it is not reasonable to detect a flaw based on the amplitude of measured signals.
- EMAR signals enable directly evaluation of the thickness of the target as demonstrated above. Thus, it is reasonable that the presence of wall thinning is evaluated basically whether the estimated depth of target is thinner than its designed thickness. That is, it is reasonable to consider not the amplitude of the measured signals but estimated depth of corrosion as $\hat{a}$.
- Usually the backwall echo when there is corrosion is sufficiently clear to evaluate the thickness of the pipe wall accurately. In contrast, it is very likely that the roughness of the surface pipe wall increases with corrosion growth, and thus the estimated depth of corrosion, $\hat{a}$, tends to differ from the true one with a as the result in Fig. ~~65~~ shows. Note that this makes it difficult to satisfy the homogeneity of variance that the conventional procedure requires.

Only a few recent studies have reported the application of POD concept to analyze EMAR signals due to wall thinning[21][22]. They transform $\hat{a}$ and a using log function so that they show a linear relationship with homogeneity, like typical POD analysis of eddy current signals. However, log transform is not preferable because it hampers to consider a=0 although EMAR, as well as the conventional ultrasonic thickness gage, would be capable of measuring the pipe thickness quite accurately.

To address the points above, this study proposes assuming that the estimated depth of corrosion, $\hat{a}$, is represented as a function of its true depth, a, as

$$\hat{a} = N(\mu_1, {\sigma_1}^2)a + N(0, {\sigma_2}^2) = N(\mu_1 a, {\sigma_1}^2 a^2 + {\sigma_2}^2),$$

where $N(\mu,\sigma^2)$ stands for a normal distribution with a mean of μ and standard deviation of σ. The mean of the second normal distribution was set to zero to take into account the fact that usually the speed of sound is evaluated according to signals due to samples without any corrosion. The three parameters, μ_1, σ_1, σ_2, can be evaluated by maximizing the following log likelihood function:

$$\ln L = -\sum_{i=1}^{N} \left\{ \frac{(\hat{a}_i - (\mu_1 a_i))^2}{2({\sigma_1}^2 {a_i}^2 + {\sigma_2}^2)} + \log\left(\sqrt{{\sigma_1}^2 {a_i}^2 + {\sigma_2}^2}\right) \right\},$$

where subscript i denotes the i-th measured data and N represents the total number of the data. Then, the probability of detection is calculated as a probability that $\hat{a}$ will exceed a given threshold $\hat{a}_{dec}$ as

$$POD(a) = \Phi\left(\frac{\mu_1 a - \hat{a}_{dec}}{\sqrt{{\sigma_1}^2 {a_i}^2 + {\sigma_2}^2}}\right)$$

like the conventional procedure. The confidence interval of the probability of detection can be calculated using the bootstrap method[23]. It is possible that in reality not only the depth but also other parameters, such as the width of corrosion, would affect the probability of detection. However, as this study did not confirm a clear correlation between the width and $\hat{a}$, the proposed model avoided taking multiple parameters into consideration [24]-[27].

Figure ~~7~~10 shows the relationship between $\hat{a}$ and a evaluated by the proposed model together with that evaluated by the conventional one. The figure clearly shows that the proposed model well represents the characteristics of the EMAR signals. That is, the error in estimating the depth of corrosion tends to increase with the depth. The gradient of the solid line is approximately 1.0 in both cases, which is reasonable because $\hat{a}$ and a are in the same dimension with the same unit. It should be noted that in the conventional model one standard deviation at a=0 exceeds $\hat{a}$=0.5. This indicates that evaluating the detectability of EMAR using the conventional model would lead to a false positive rate of more than 16% even if setting $\hat{a}_{dec}$=0.5, which is obviously unrealistic. In contrast, one standard deviation at a=0 is less than 0.2 in the proposed model, indicating that $\hat{a}_{dec}$=0.5 would lead to very little possibility of a false positive. Actually, the experiments using the seven samples with no corrosion to estimate v showed that the standard deviation and the maximum of evaluated depth of corrosion using the estimated v were 0.039 and 0.094 mm, respectively.

Figures ~~8~~11 and ~~9~~12 show the probability of detection curves when $\hat{a}_{dec}$ was set to 0.2, 0.5, 1.0 and 2.0 mm, obtained by the conventional and proposed model respectively. The solid and dashed curves in the figures represent POD as a function of flaw depth and its 95% confidence bounds, respectively. The figures present two parameters commonly used to characterize the probability of detection: a_{50}, the size of a flaw having a 50% probability of detection as an asterisk, and $a_{90/95}$, the minimum size of a flaw that can be detected in 90% of cases with 95% confidence as a filled circle. The figures demonstrate that the two models provide similar POD curves when $\hat{a}_{dec}$ is as large as 2.0 mm. In contrast, their discrepancy becomes larger at smaller $\hat{a}_{dec}$, indicating the effectiveness of the proposed model in evaluating the capability of EMAR in detecting initial wall thinning. Specifically, for example, Fig. 6 indicates that it is unlikely that a flaw with a depth of 0.5 mm is evaluated to have a depth of deeper than 1 mm. Thus, if $\hat{a}_{dec}$ is set to 1.0 mm, POD at a = 0.5 mm should be quite small. The POD obtained by the conventional model overestimates the POD; whereas the one by the proposed model reflect this more reasonably. Figure ~~10~~13 presents how $\hat{a}_{dec}$ affects the false positive rate and the two parameters characterizing the probability of detection. The figure also supports the superiority of the proposed model if one needs to detect wall thinning in its early stages.

4. Conclusion

This study proposed a POD model taking account of the characteristics of EMAR to detect and evaluate pipe wall thinning due to FAC. One of main differences between the proposed model and conventional one is that the proposed one can reasonably represent such characteristics of EMAR signals that the error in evaluating the depth of corrosion tends to increase with the depth. Analyzing EMAR signals due to artificial corrosion introduced into carbon steel plates confirmed that the proposed model is able to evaluate the probability of detection against shallow corrosion, as well as the false positive rate, more reasonably than the conventional POD model.

References

[1] H. Yun, S.J. Moon, Y.J. Oh, Development of wall-thinning evaluation procedure for nuclear power plant piping -- Part 1: Quantification of thickness measurement deviation, Nuclear Engineering and Technology 48 (2016), 820-830.

[2] K. Kawashima, O.B. Wright, Resonant electromagnetic excitation and detection of ultrasonic waves in this sheets, Journal of Applied Physics 72 (1992), 4830.

[3] M. Hirao, H. Ogi, H. Fukuoka, Resonance EMAT system for acoustoelastic stress measurement in sheet metals, Review of Scientific Instruments 64 (1993), 3198.

[4] K. Kawashima, T. Hyoguchi, T. Akagi, On-line measurement of plastic strain ratio of steel sheet using resonance mode EMAT, Journal of Nondestructive Evaluation 12 (1993), 71-77.

[5] H. Ogi, M. Hirao, T. Honda, Ultrasonic attenuation and grain-size evaluation using electromagnetic acoustic resonance, The Journal of the Acoustical Society of America 98 (1995), 458-464.

[6] S. Dixon, C. Edwards, S.B. Palmer, High accuracy non-contact ultrasonic thickness gauging of aluminium sheet using electromagnetic acoustic transducers, Ultrasonics 39 (2001), 445-453.

[7] A. Tagawa, K. Fujiki, F. Kojima, Investigation of the on-line monitoring sensor for a pipe wall thinning with high accuracy, E-Journal of Advanced Maintenance 1 (2009), 52-62.

[8] R. Urayama, T. Uchimoto, T. Takagi, S. Kanemoto, Quantitative evaluation of pipe wall thinning by electromagnetic acoustic resonance, E-Journal of Advanced Maintenance 2 (2010/2011), 25-33.

[9] D. Kosaka, F. Kojima, H. Yamaguchi, K. Umetani, Monitoring system for pipe wall thinning management using electromagnetic acoustic transducer, E-Journal of Advanced Maintenance 2 (2010/2011), 34-42.

[10] R. Urayama, T. Takagi, T. Uchimoto, S. Kanemoto, Online monitoring of pipe wall thinning by electromagnetic acoustic resonance method, E-Journal of Advanced Maintenance 5 (2013), 155-164.

[11] T. Takagi, R. Urayama, T. Ichihara, T. Uchimoto, T. Ohara, T. Kikuchi, Field application of electromagnetic acoustic resonance to inspection of pipe wall thinning in a nuclear power plant, Electromagnetic Nondestructive Evaluation (XVI), pp. 312-318, J.M.A. Rebello et al. (Eds.), IOS Press, 2014.

[12] H. Sun, R. Urayama, F. Kojima, M. Hashizmoto, T. Uchimoto, T. Takagi, Comparative study of continuous wave and pulse wave electromagnetic acoustic resonance for the measurement of pipe wall thickness, Journal of Japan Society of Applied Electromagnetics and Mechanics 26 (2018), 312-319.

[13] Department of Defense Handbook: Nondestructive Evaluation System Reliability Assessment: USDOD, MIL-HDBK-1823A, 2009.

[14] C. Annis, J.C. Aldrin, A. Sabbagh, “NDT Capability - What is missing in nondestructive testing capability evaluation?” Materials Evaluation, vol. 73, no. 3, pp. 44-54, 2015.

[15] A.P. Berens, NDE Reliability data analysis, ASM Handbook, Volume 17: Nondestructive Evaluation and Quality Control: ASM International, pp. 689-670, 1989.

[16] N. Dominguez, V. Feuillard, F. Jenson, P. Willaume, Simulation assisted pod of a phased array ultrasonic inspection in manufacturing, AIP Conference Proceedings 1430 (2012), 1765.

[17] S.M. Subair, K. Balasubramaniam, P. Rajogopal, A. Kumar, B.P. Rao, T. Jayakumar, Finite element simulations to predict probability of detection (PoD) curves for ultrasonic inspection of nuclear components, Procedia Engineering 86 (2014), 461-468.

[18] V.K. Rentala, P. Mylavarapu, J.P. Gautam, Issues in estimating probability of detection of NDT technique - A model assisted approach, Ultrasonics 87 (2018), 59-70.

[19] P.N. Bilgunde, L.J. Bond, Monde-assisted approach for probability of detection (POD) in high-temperature ultrasonic NDE using low-temperature signals, Nuclear Technology 202 (2018), 161-172.

[20] M.S.S.A. Ali, A. Kumar, P.B. Rao, J. Tammana, K. Balasubramanian, P. Rajagopal, Baysian synthesis for simulation-based generation of probability of detection (PoD) curves, Ultrasonics 84 (2018), 210-222.

[21] H. Nakamoto, F. Kojima, H. Tabata, D. Kosaka, Reliability evaluation of pipe thickness measurement by electromagnetic acoustic transducer, International Journal of Applied Electromagnetics and Mechanics 45 (2014), 923-929.

[22] H. Nakamoto, F. Kojima, S. Kato, Reliability assessment for thickness inspection of pipe wall using probability of detection, E-Journal of Advanced Maintenance 5 (2014), 228-237.

[23] J.S. Knopp, R. Grandhi, J.C. Aldrin, I. Park, Statistical analysis of eddy current data from fastener site inspections, Journal of Nondestructive Evaluation 32 (2013), 44-50.

[24] M. Pavlovic, K. Takahashi, C. Muller, Probability of detection as a function of multiple influencing parameters, Insight 52 (2012), 606-611.

[25] N. Yusa, J. Knopp, Evaluation of Probability of Detection (POD) studies with multiple explanatory variables, Journal of Nuclear Science and Technology 53 (2016), 574-579.

[26] N. Yusa, W. Chen, H. Hashizume, Demonstration of probability of detection taking consideration of both the length and the depth of a flaw explicitly, NDT&E International 81 (2016), 1-8.

[27] A. Gianneo, M. Carboni, M. Giglio, Feasibility study of a multi-parameter probability of detection formulation for a Lamb waves-based structural health monitoring approach to light alloy aeronautical plates, Structural Health Monitoring 16 (2017), 225-249.

[28] J.H. Kurz, A. Jungert, S. Dugan, G. Dobmann, C. Boller, Reliability consideration of NDT by probability of detection (POD) determination using ultrasound phased array, Engineering Failure Analysis 35 (2013), 609-617.

List of Figures

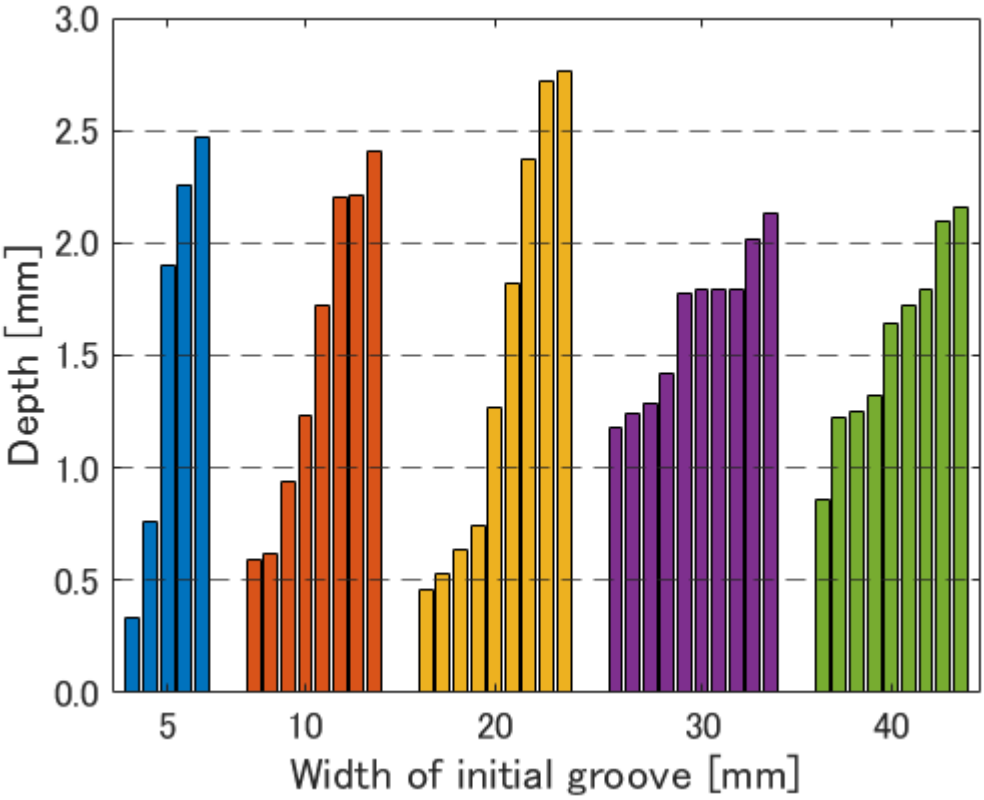

Figure 1 The depths and the initial widths of grooves

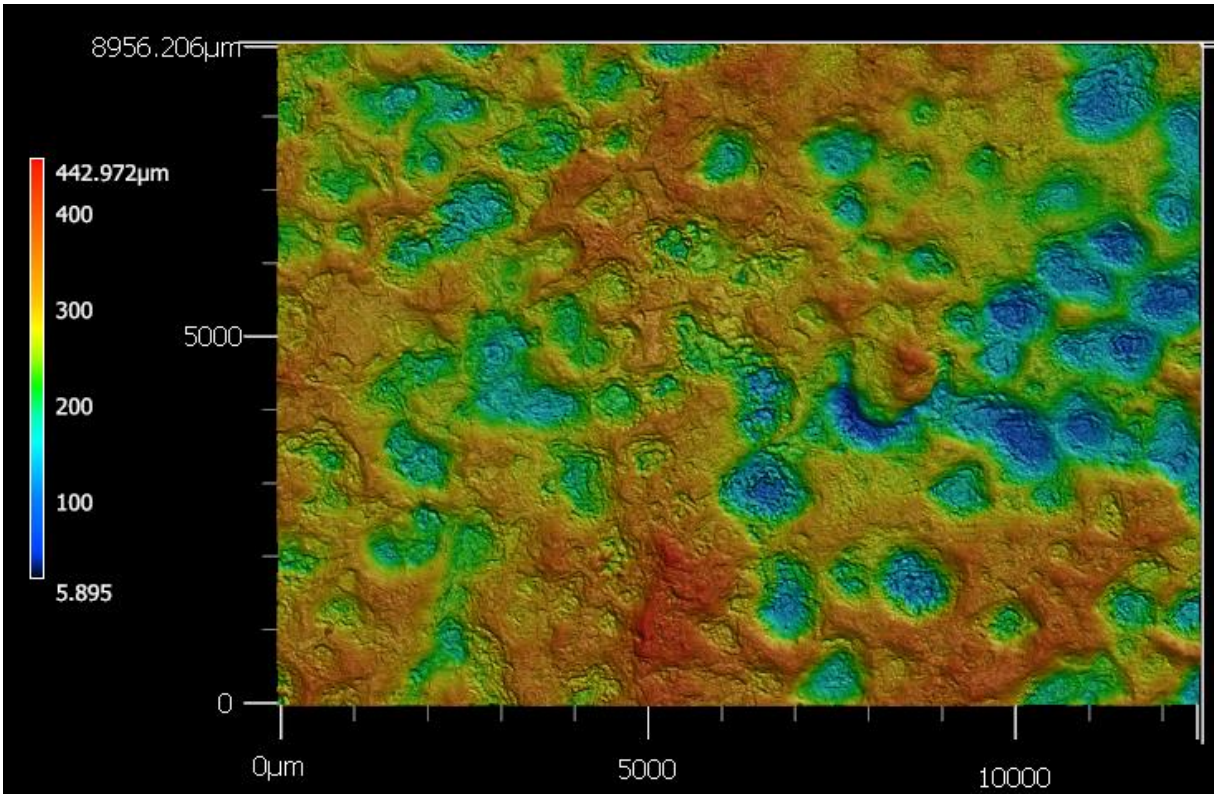

Figure 2 Microscopic picture of the surface of a groove

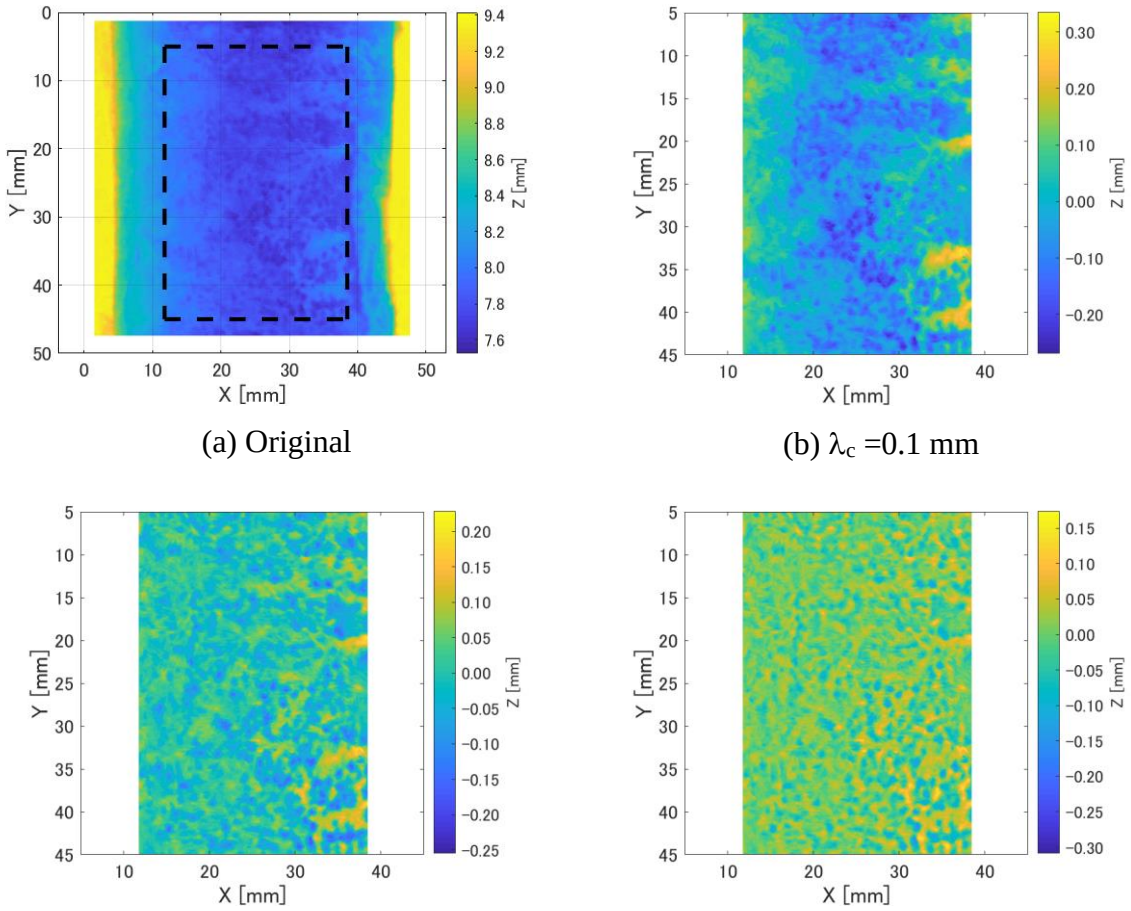

(a) Original (b) λ_c =0.1 mm

(c) λ_c=0.5 mm (d) λ_c =1.0 mm

Figure 3 Measured height of samples (a), and their high frequency components with different cut-off wavelength, λc (b)-(d). The broken lines in (a) shows the area used for the further evaluations. To avoid the effect of the profile of the initial groove, the evaluations considered 2/3 in the X direction and excluded several millimeters in the Y direction

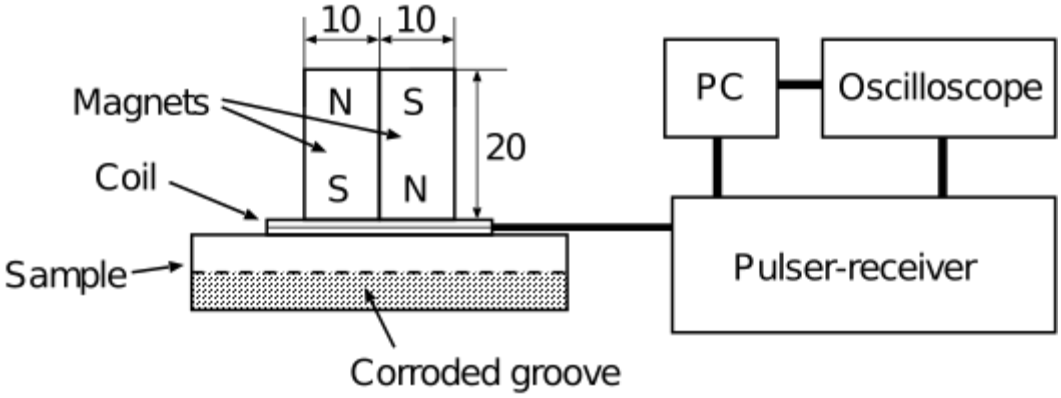

(a) Experimental setup

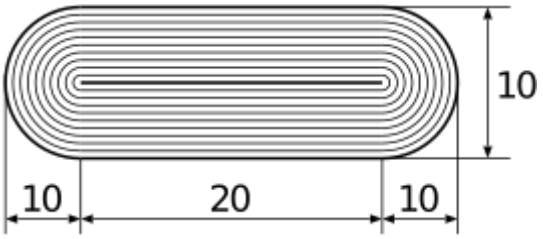

(b) coil profile

Figure 4 Experimental setup (a) and coil for the EMAR probe (b) used in this study (unit: mm)

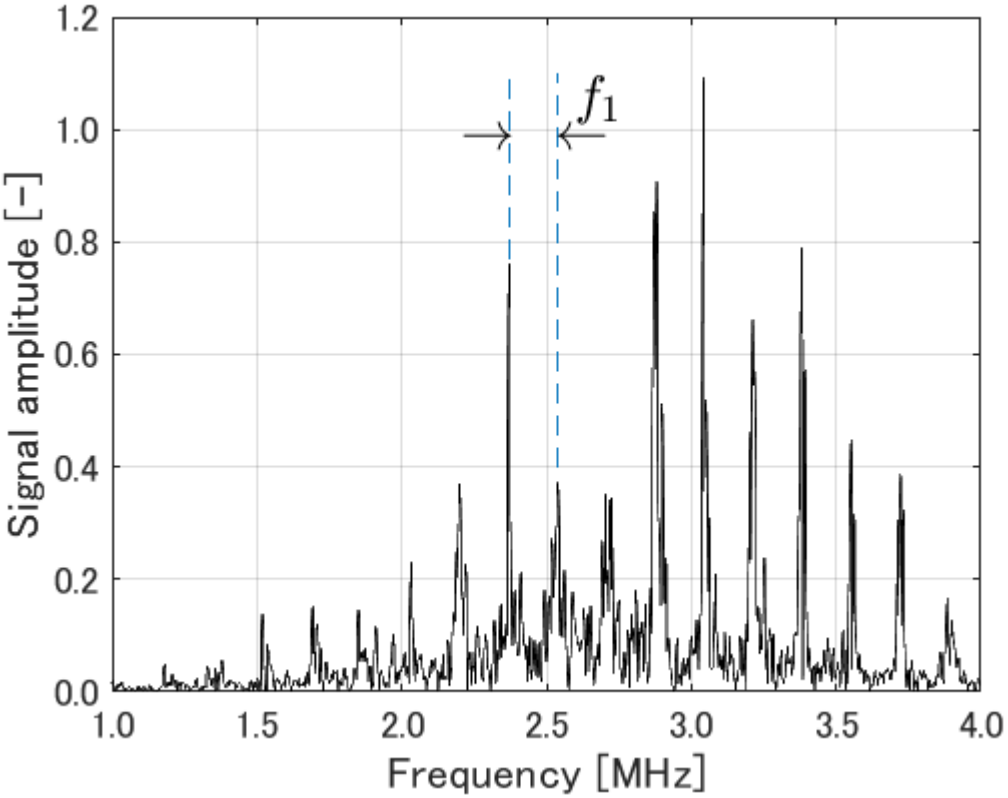

Figure 5 Measured EMAR signals

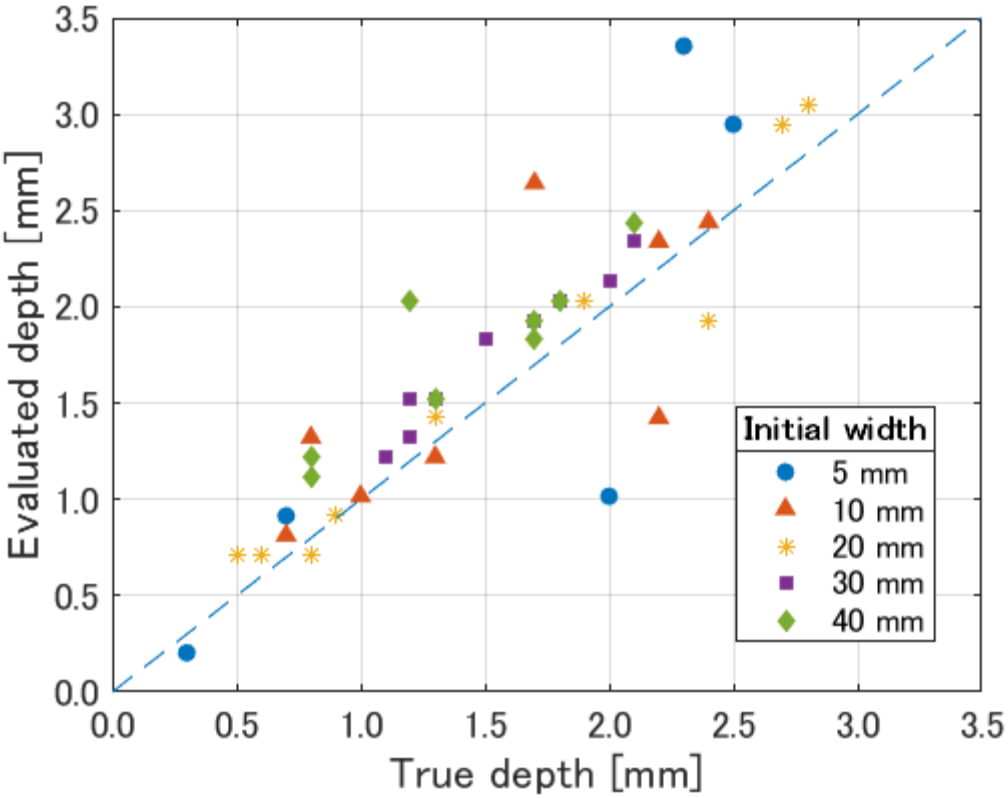

Figure 6 Comparison between true and estimated depths.

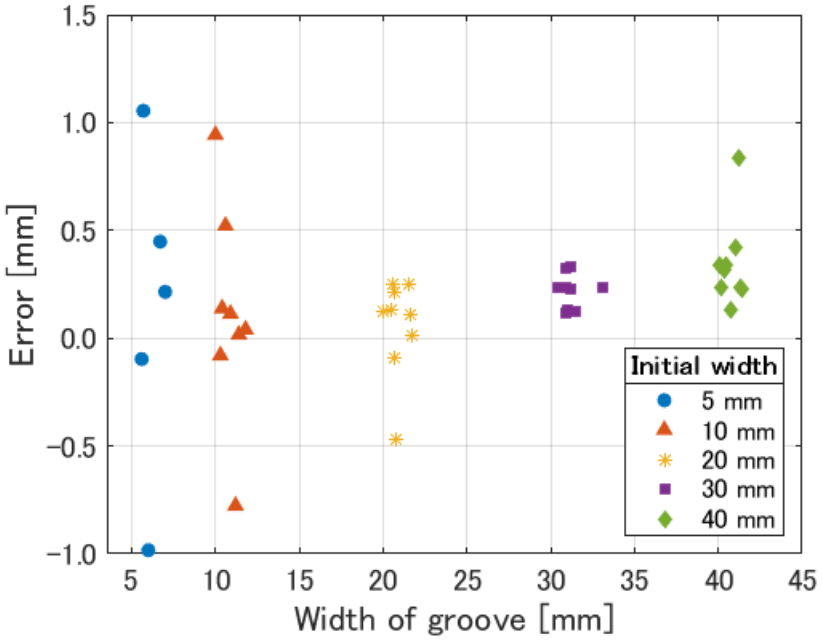

(a) absolute error

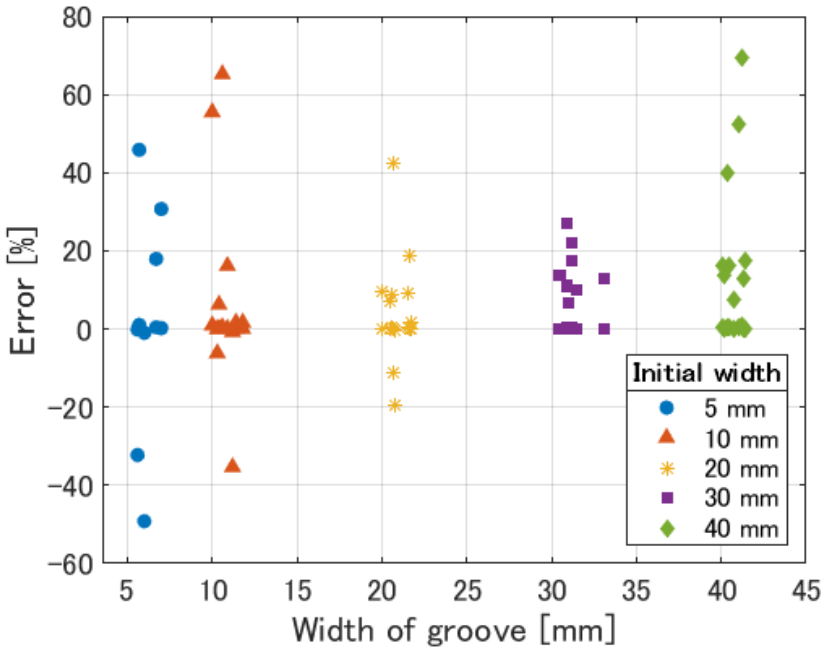

(b) relative error

Figure 7 The relationships between the width of groove and the error in evaluating the depths of the grooves

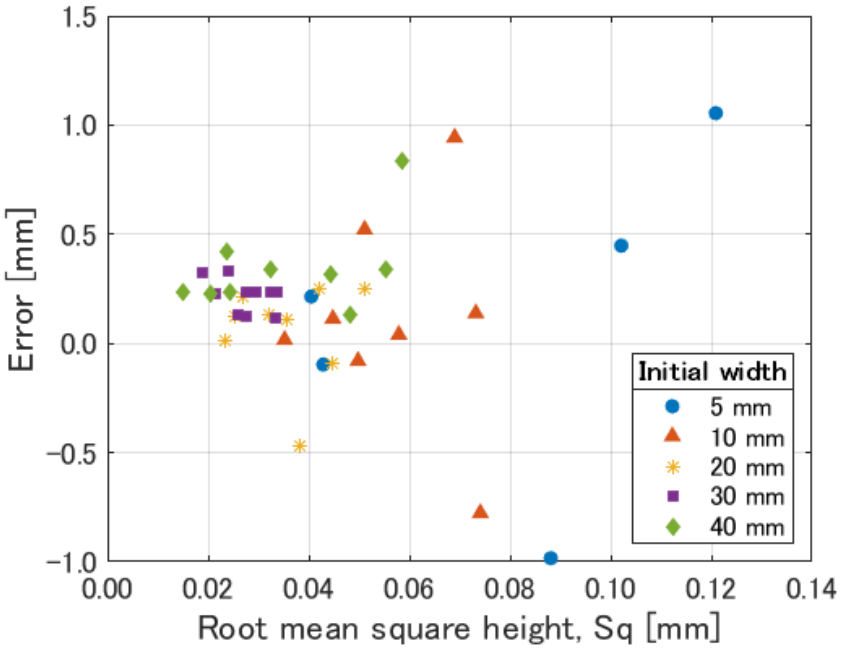

(a) absolute error

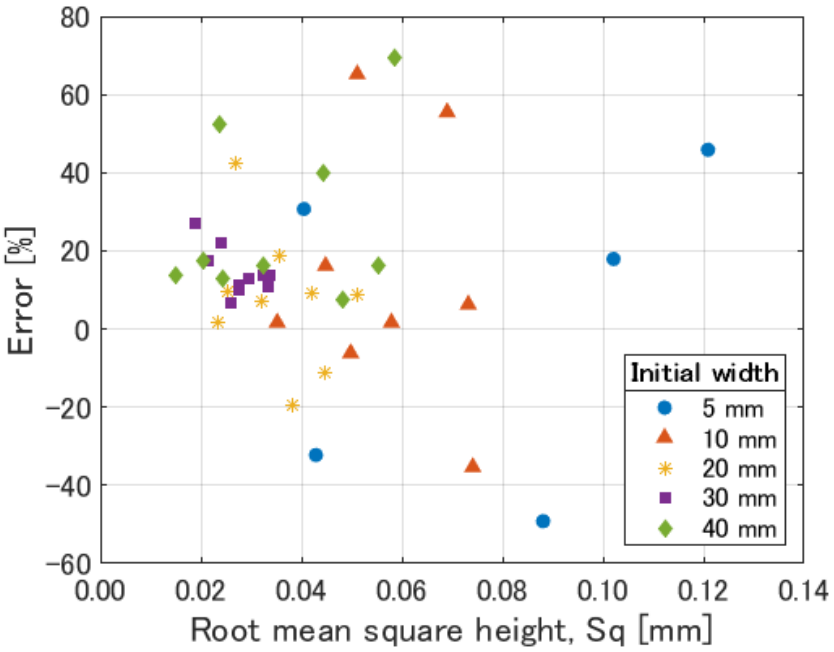

(b) relative error

Figure 8 The relationship between the root mean square height and the error in evaluating the depth

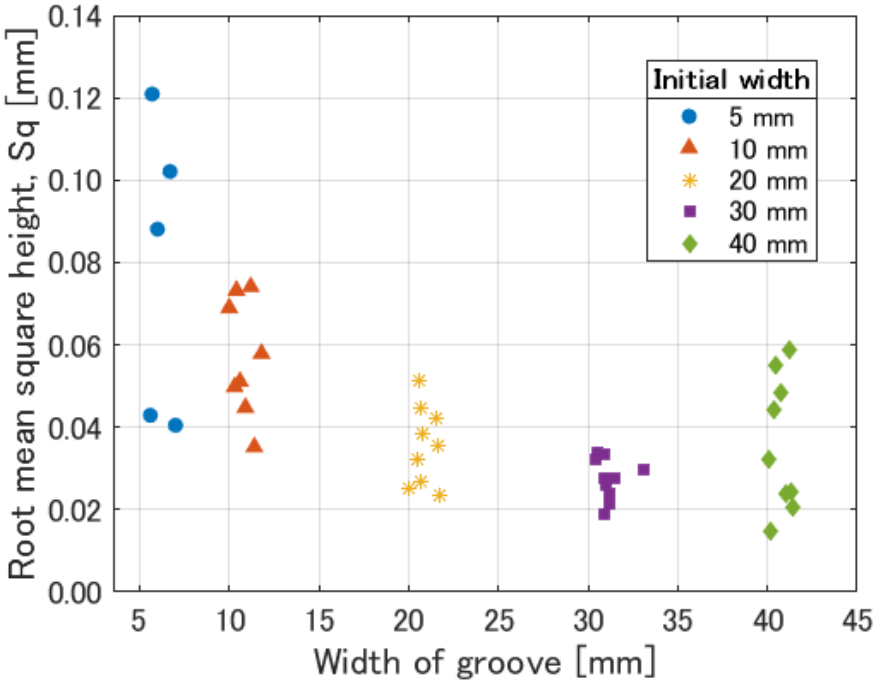

Figure 9 The relationships between the width of groove and root mean square height

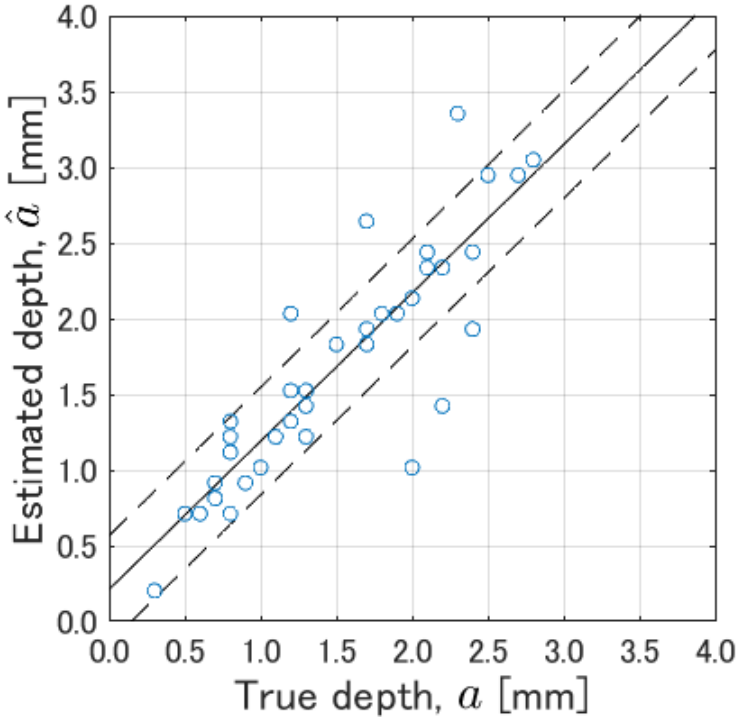

(a) conventional model

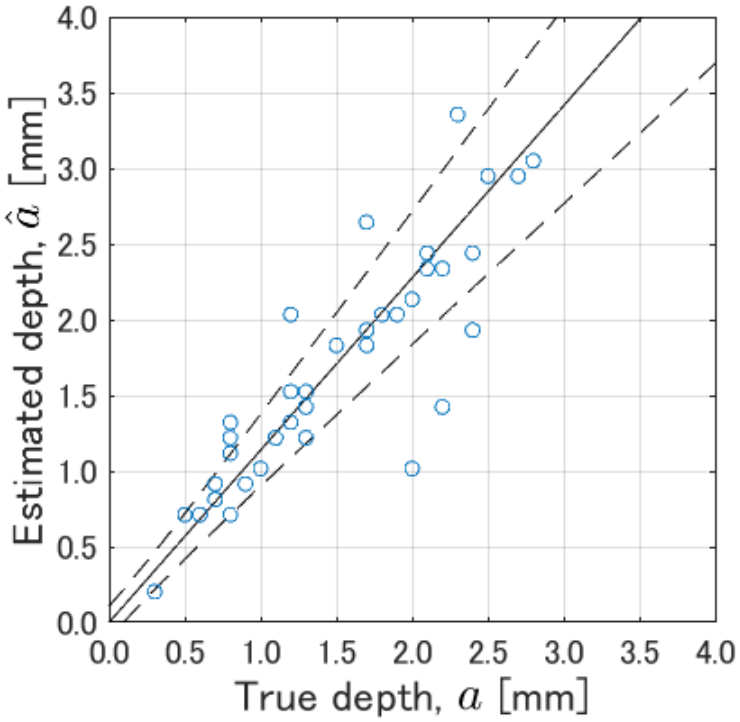

(b) proposed model

Figure 10 Results of regression analyses. Solid and broken lines correspond to the mean and mean± standard deviation, respectively.

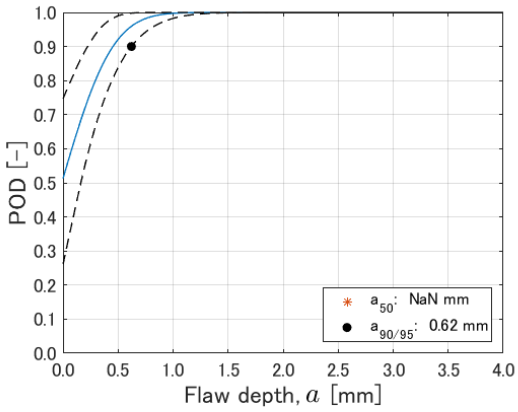

(a) $\hat{a}_{\mathrm{dec}}$=0.2 mm

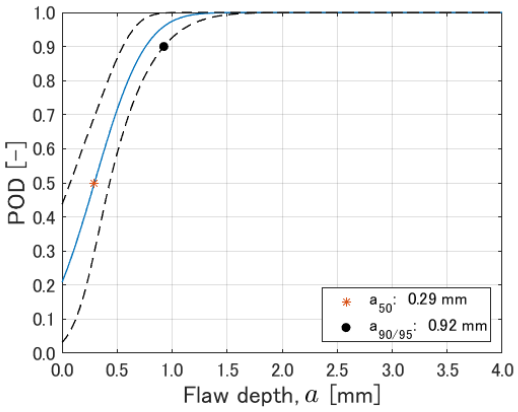

(b) $\hat{a}_{\mathrm{dec}}$=0.5 mm

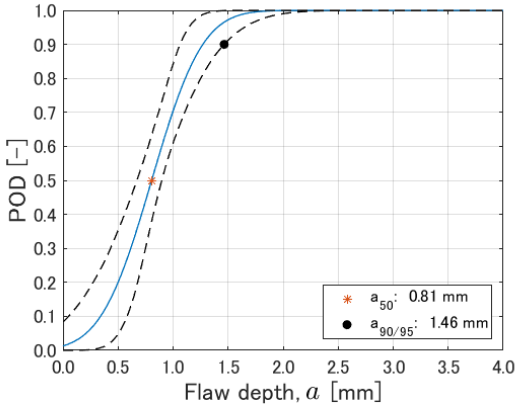

(c) $\hat{a}_{\mathrm{dec}}$=1.0 mm

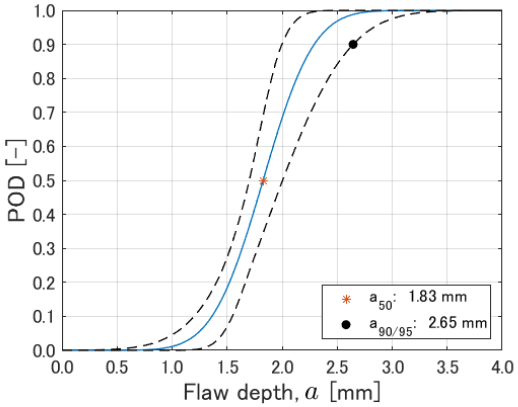

(d) $\hat{a}_{\mathrm{dec}}$=2.0 mm

Figure 11 POD curves based on the conventional model

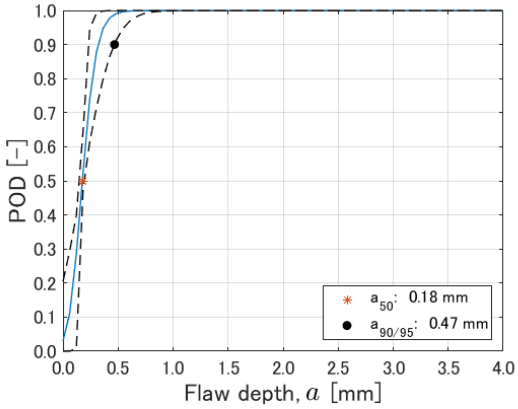

(a) $\hat{a}_{dec}$=0.2 mm

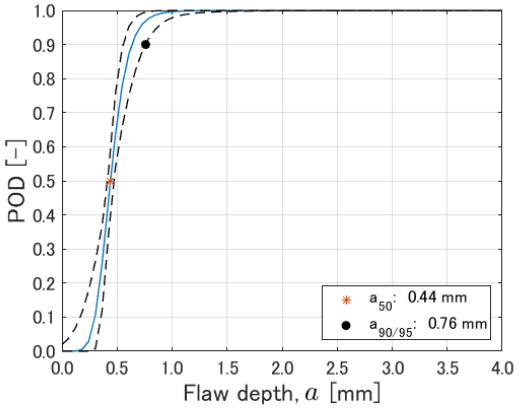

(b) $\hat{a}_{dec}$=0.5 mm

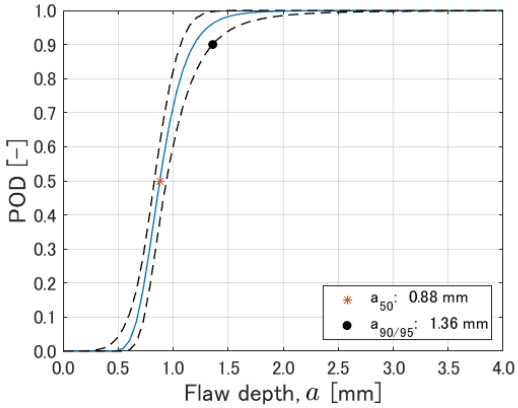

(c) $\hat{a}_{dec}$=1.0 mm

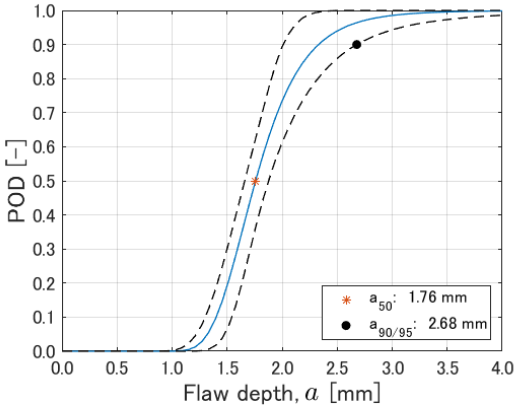

(d) $\hat{a}_{dec}$=2.0 mm

Figure 12 POD curves based on the proposed model

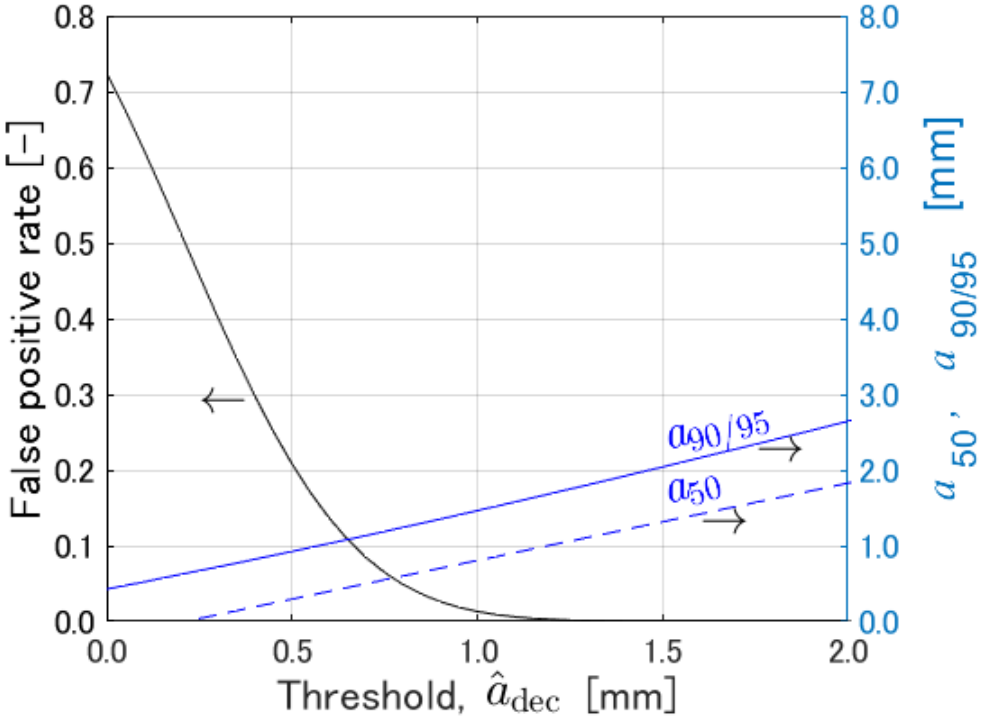

(a) conventional model

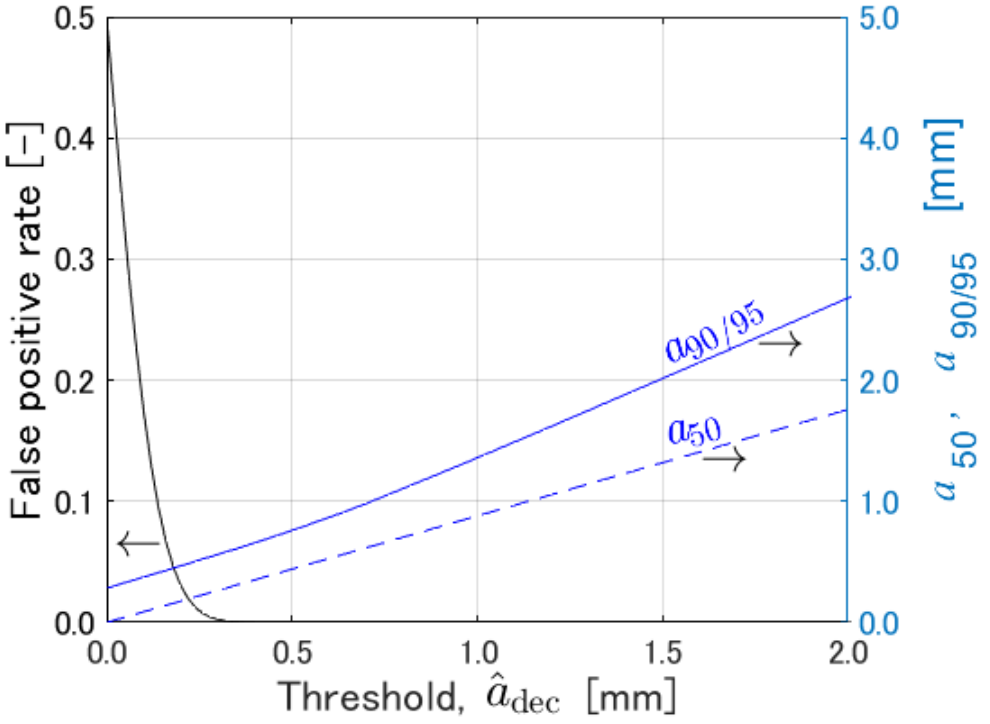

(b) proposed model

Figure 13 Effect of the threshold, $\hat{a}_{\mathrm{dec}}$, on false positive and detectability.